Inorganic Chemistry

pubs.acs.org/IC

Article

Concentration-Quenching-Suppressed Eu^{3+}-Activated $Ba_3Lu_2B_6O_{15}$ Orange-Red-Emitting Phosphors via One-Dimensional Structural Confinement for Thermally Stable White LEDs

Shengtao Ren, Ximing Kong, Mingpan Wei, Ziyao Wang,* Yangai Liu,* Benjamin Dierre, Ruben Abellon, and H. T. Hintzen*

Cite This: *Inorg. Chem.* 2025, 64, 18588−18598

Read Online

ACCESS | Metrics & More | Article Recommendations | Supporting Information

ABSTRACT: Conventional Eu^{3+}-activated phosphors often suffer from severe concentration quenching at high doping levels, significantly limiting their achievable brightness and efficiency. Furthermore, achieving both high color purity and strong emission intensity in the orange-red region remains challenging. In this context, we report the successful synthesis of Eu^{3+}-activated $Ba_3Lu_2B_6O_{15}$ phosphors via a multistep solid-state reaction under ambient conditions, exhibiting intense reddish-orange emission. Upon near-ultraviolet excitation at 398 nm, the phosphors exhibited dominant emission at 593 nm with a long decay time (about 4.1 ms), attributed to the magnetic dipole-allowed $^5D_0 \rightarrow {}^7F_1$ transition of Eu^{3+} ions occupying inversion-symmetric Lu^{3+} lattice sites. Remarkably, concentration quenching of Eu^{3+} luminescence in $Ba_3Lu_{2(1-x)}Eu_{2x}B_6O_{15}$ was completely suppressed even at 70 mol % Eu^{3+} doping ($x = 0.70$), which can be understood from the unique one-dimensional chain-like architecture of the host lattice that restricts inter-Eu^{3+}-ion energy migration to defect states. The as-synthesized $Ba_3Lu_{0.6}Eu_{1.4}B_6O_{15}$ composition demonstrated an internal quantum efficiency of ∼53%, coupled with superior color purity (97.5%) as evidenced by CIE coordinates of (0.605, 0.387). Furthermore, the material displayed outstanding thermal stability, retaining ∼98% of its room-temperature emission intensity at 450 K. These combined attributes position $Ba_3Lu_2B_6O_{15}$:Eu^{3+} as a promising phosphor for next-generation warm-white LEDs.

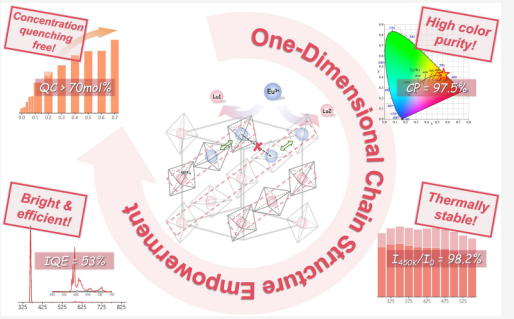

1. INTRODUCTION

White light-emitting diodes (*w*-LEDs) have been proved to be an ideal substitute for traditional light sources and have been widely commercialized in the fields of lighting and display because of their features of small volume, low power consumption, long working lifetime, short response time, and environmental friendliness.[1−4] Currently, most industrial *w*-LEDs are the combination of an InGaN chip emitting blue light and a yellow-emitting yttrium aluminum garnet (YAG) conversion phosphor doped with trivalent Ce^{3+}, by which part of the blue light is converted into yellow light. But, as we know, this type of *w*-LED usually suffers from a poor color rendering index (CRI < 75) and a correlated color temperature (CCT) higher than 4000 K caused by the color deficiency in the red region, which has hampered its popular application, especially in interior illumination.[5,6]

For resolving this problem, many attempts and progresses have been made during the last few decades. At first, sulfide phosphors such as CaS:Eu^{2+}[7] and subsequently nitride phosphors, such as $Sr_2Si_5N_8$:Eu^{2+}[8,9] and $CaAlSiN_3$:Eu^{2+},[10] were invented as the red-emitting components for white LED applications. Meanwhile, YAG:Ce^{3+} was combined with the red-emitting K_2SiF_6:Mn^{4+} phosphor,[11,12] which turned out to be considerably vulnerable to moisture. Another feasible method is to combine phosphors emitting red−green−blue (RGB) light with a near-ultraviolet (n-UV) LED chip to achieve white light emission; among them, the red (orange)-emitting phosphor plays an irreplaceable role in reducing the CCT of white light and improving its color rendering.[7,13] However, the present red-emitting phosphors still have difficulty meeting actual application requirements. For example, the conventional red-emitting phosphors, including Eu^{2+}-doped sulfides (e.g., CaS:Eu^{2+})[7] and Eu^{3+}-doped oxysulfides (e.g., Y_2O_2S:Eu^{3+}),[14,15] generally suffer from low quantum efficiency and poor chemical and thermal stability. Also, a maximum luminous efficacy of a broad red emission band from Eu^{2+} cannot be expected, possibly except for a few relatively narrow-band emitting phosphors, such as $SrLiAl_3N_4$:Eu^{2+} (with Eu^{2+} on a very symmetric site), because generally the broadband $4f^65d^1 \rightarrow 4f^7$ red Eu^{2+} emission with

Received: July 23, 2025
Revised: August 12, 2025
Accepted: August 25, 2025
Published: September 2, 2025

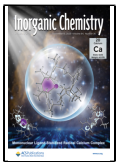

an fwhm >70 nm extends to longer wavelengths where the human eye is insensitive.[16]

However, red line emission enables the combination of high luminous efficiency with a high color rendering index. Eu^{3+} can be a good candidate for avoiding the extension of unwanted emission in the near-infrared region because it presents typical narrow emissions due to 4f−4f transitions in the orange ($^5D_0 \rightarrow {}^7F_1$) or red ($^5D_0 \rightarrow {}^7F_2$) region, with the dominant emission depending on the site symmetry.[17] Therefore, researchers have been trying to find suitable host materials and develop new Eu^{3+}-activated phosphors with sufficient narrow red (orange) emission. The chromaticity coordinates and internal quantum efficiency of several reported Eu^{3+}-activated phosphors are listed in Table 1, from which we can see that high efficiencies can be obtained.

Table 1. Chromaticity Coordinates and Internal Quantum Efficiency of Various Reported Eu^{3+}-activated Red (Orange)-Emitting Phosphors

Phosphors	Excitation maximum (nm)	Dominant emission (nm)	Chromaticity coordinates (x, y)	IQE (%)	ref.
$Y_2O_3:Eu^{3+}$	230	611 ($^5D_0 \rightarrow {}^7F_2$)	(0.66, 0.34)	92	[18,19]
$Y_2O_2S:Eu^{3+}$	394	614 ($^5D_0 \rightarrow {}^7F_2$)	(0.65, 0.35)	91	20
$(Y,Gd)BO_3:Eu^{3+}$	250	590 ($^5D_0 \rightarrow {}^7F_1$)	(0.64, 0.35)	74	21
$YVO_4:Eu^{3+}$	318	618 ($^5D_0 \rightarrow {}^7F_2$)	(0.66, 0.34)	70	22

During the last decades, borates, as a type of host lattice material, have generated broad interest and attention due to their high chemical stability, low synthesis temperature, and large bandgap.[23,24] Rare-earth-doped borate phosphors have been widely studied and used for different applications, such as $GdMgB_5O_{10}:Ce^{3+}$, Tb^{3+} as a green-emitting component in tricolor fluorescent lamps,[25] green-emitting $(Y,Gd)BO_3:Tb^{3+}$ phosphors for plasma displays,[26] and $InBO_3:Tb^{3+}$ as a green-emitting phosphor for projection television cathode-ray tubes.[27]

More recently, the luminescence of a novel borate lattice $Ba_3Ln_2B_6O_{15}:M^{3+}$ (Ln = Y, Lu) doped with M = Ce, Tb, and Eu has been reported. The luminescence properties of Ce^{3+}-doped $Ba_3Lu_2B_6O_{15}$ have been studied by Li et al.[28] They synthesized Ce^{3+}-activated $Ba_3Lu_2B_6O_{15}$ blue-emitting phosphors with a narrow fwhm (68 nm) of the blue emission band (with peak emission at about 440 nm) due to the highly symmetric local environment of the $[CeO_6]$ octahedron. The studied phosphor $Ba_3Lu_2B_6O_{15}:0.03Ce^{3+}$ presented a high internal quantum efficiency of 71%. Huang et al.[29] doped Ce^{3+} and Tb^{3+} together into the host lattice $Ba_3Lu_2B_6O_{15}$ and got a high $Ce^{3+}-Tb^{3+}$ energy-transfer efficiency of 62% and a corresponding IQE of 51%. Annadurai et al.[30] reported the isostructural Eu^{3+}-activated $Ba_3Y_2B_6O_{15}$ phosphor, in which Eu^{3+} ions occupy the Y-sites with inversion symmetry and emit bright reddish-orange emission. The resulting IQE was measured to be only 13%. Inspired by these developments, we initiated an independent investigation into the photoluminescence properties of Eu^{3+}-doped $Ba_3Lu_2B_6O_{15}$. Notably, while Kolesnikov et al.[31] concurrently reported on this phosphor system, our work provides a groundbreaking perspective by revealing the complete suppression of concentration quenching at an unprecedented 70 mol % Eu^{3+} doping. This exceptional behavior is mechanistically linked to the unique one-dimensional chain-like architecture of the host lattice, which fundamentally restricts interion energy migration. Furthermore, our study offers the first comprehensive analysis of site-symmetry-dependent luminescence dynamics and thermal stability in this system, supported by rigorous structural refinement and quantum efficiency measurements. These insights not only resolve long-standing limitations in high-concentration Eu^{3+} phosphor design but also position $Ba_3Lu_2B_6O_{15}:Eu^{3+}$ as a transformative candidate for high-brightness, thermally stable w-LEDs.

2. EXPERIMENTAL DETAILS

$Ba_3Lu_{2(1-x)}Eu_{2x}B_6O_{15}$ phosphors with different Eu^{3+} concentrations were synthesized by a multistep solid-state reaction in air with starting materials $BaCO_3$ (3N), Lu_2O_3 (3N), Eu_2O_3 (4N), and 3 wt % excess of H_3BO_3 (3N). All chemicals used were purchased from Sigma-Aldrich and used without further purification. Stoichiometric amounts of raw materials were thoroughly mixed and homogenized in an agate mortar, and all samples were heated in corundum crucibles in air at 900 °C for 12 h, then ground, and fired once more at 910 °C for 12 h. The obtained samples were naturally cooled to room temperature and ground for further characterization.

The phase formation of the synthesized samples was studied by X-ray diffraction (XRD) on a PANalytical X'Pert PRO X-ray diffraction system with Cu Kα1 radiation (λ = 1.5406 Å) at a tube voltage of 45 kV and a tube current of 30 mA (step size = 0.02°, counting time per step = 25 s, corresponding to a scan rate of 0.048°/min). The powder XRD pattern for Rietveld analysis was collected with the same system (step size = 0.008°, counting time per step = 45 s, corresponding to a scan rate of 0.01°/min), and the Rietveld refinement was performed by using the TOPAS program. The photoluminescence emission (PL) and excitation (PLE) spectra were measured with equipment utilizing a xenon lamp, a Horiba Gemini 180 monochromator, a PerkinElmer MP-1913 photomultiplier (PMT), and a Lake Shore 331 temperature controller. The thermoluminescence (TL) glow curves were collected on an LTTL-3DS TL spectrometer. The phosphor sample was exposed to X-ray irradiation at 30 kV for 5 min, followed by heating at a constant rate of 5 °C/s. The internal quantum efficiency (IQE) was measured at room temperature on an Edinburgh FLS980 fluorescence spectrophotometer equipped with Hamamatsu R982P visible photomultiplier tube detectors. The internal quantum efficiency of $Ba_3Lu_{2(1-x)}Eu_{2x}B_6O_{15}$ was calculated based on the following equation:

$$\mathrm{IQE} = \frac{\int L_S}{\int E_R - \int E_S} \times 100\% \quad (1)$$

Here, L_S refers to the integrated emission spectrum of the $Ba_3Lu_{2(1-x)}Eu_{2x}B_6O_{15}$ sample; E_S and E_R are the integrated intensities of the excitation radiation reflected to the $Ba_3Lu_{2(1-x)}Eu_{2x}B_6O_{15}$ sample and $BaSO_4$ reference, respectively. For LED tests, the $Ba_3Lu_{2(1-x)}Eu_{2x}B_6O_{15}$ phosphor was mixed with the commercial blue-emitting $BaMgAl_{10}O_{17}:Eu^{2+}$ (BAM:Eu^{2+}) phosphor and the green-emitting $Zn_2SiO_4:Mn^{2+}$ (ZSO:Mn^{2+}) phosphor, along with epoxy resin, and then coated onto a 365 nm UV chip and encapsulated into an LED device. The electroluminescence (EL) characteristics of the LED were analyzed using a HopooColor HPCS-320D spectroradiometer, while thermal distribution data was captured through a Hikvision K20 infrared thermographic system.

3. RESULTS AND DISCUSSION

Phase composition and purity of as-prepared $Ba_3Lu_{2(1-x)}Eu_{2x}B_6O_{15}$ samples are determined from XRD powder patterns (Figure 1a). When the concentration of Eu^{3+} is lower than 80 mol % (x < 0.8), the XRD diffraction peaks on the patterns are consistent with each other and match

https://doi.org/10.1021/acs.inorgchem.5c03366
Inorg. Chem. 2025, 64, 18588−18598

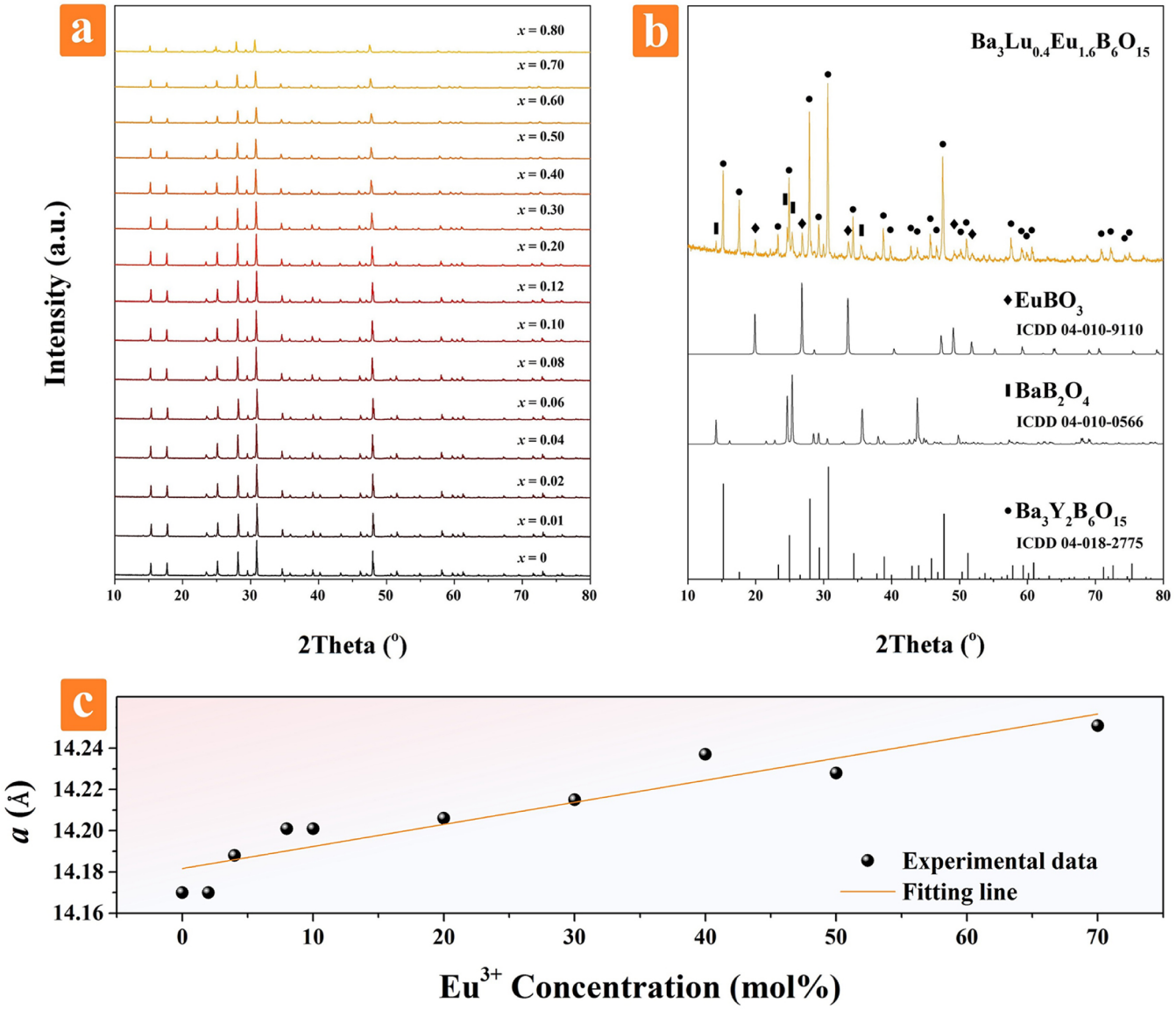

Figure 1. XRD patterns of as-synthesized $Ba_3Lu_{2(1-x)}Eu_{2x}B_6O_{15}$ samples for various Eu concentrations (a); XRD pattern of $Ba_3Lu_{0.4}Eu_{1.6}B_6O_{15}$ with standard ICDD cards at the bottom (b); the cubic lattice parameter *a* of $Ba_3Lu_{2(1-x)}Eu_{2x}B_6O_{15}$ depending on the Eu^{3+} concentration (c).

well with the standard pattern of $Ba_3Y_2B_6O_{15}$. All samples with $x < 0.8$ are in the pure $Ba_3Lu_2B_6O_{15}$ phase, indicating that the incorporation of Eu^{3+} has negligible influence on the structure of $Ba_3Lu_2B_6O_{15}$ except for the expansion of the unit cell. As shown in Figure 1b, the phases of $(Eu,Lu)BO_3$ and BaB_2O_4 appear as impurities for $x = 0.8$, indicating that the maximum solubility of Eu^{3+} in $Ba_3Lu_2B_6O_{15}$ at 910 °C has been surpassed. Figure 1c shows the increase in the cubic lattice parameter *a* for higher Eu^{3+} concentrations, indicating that the Eu^{3+} ions are more likely to occupy the smaller Lu^{3+} sites than the larger Ba^{2+} sites, as expected from the perspectives of similar ionic size and isovalency. In agreement with Vegard's law, the value of *a* shows an approximate linear trend of getting larger when the concentration of Eu^{3+} is increased up to 70 mol % due to lattice expansion when Lu^{3+} [$r(Lu^{3+}) = 0.86$ Å] was replaced by the larger Eu^{3+} [$r(Eu^{3+}) = 0.95$ Å].[32]

Figure 2a and b present the observed (black cross), calculated (red lines), and difference (bottom) XRD profiles for the Rietveld refinement results of $Ba_3Lu_2B_6O_{15}$ and $Ba_3Lu_{0.6}Eu_{1.4}B_6O_{15}$, respectively. The refinement data and fitting details are summarized in Table 2. Herein, the crystallographic parameters of isostructural $Ba_3Lu_2B_6O_{15}$ are used as initial parameters in the Rietveld analysis. Clearly, all peaks can be indexed by a cubic unit cell with space group $Ia\bar{3}$ and lattice parameters close to those of $Ba_3Lu_2B_6O_{15}$ [$a = 14.253(6)$ Å, $V = 2895(2)$ Å^3].[33] The final refinement is stable and converges well with low residual factors, demonstrating that the refined results are reliable. The smaller lattice volume of $Ba_3Lu_2B_6O_{15}$ (2836 Å^3) versus $Ba_3Lu_2B_6O_{15}$ (2895 Å^3) results from the replacement of Lu^{3+} [$r(Lu^{3+}) = 0.86$ Å] by the larger Y^{3+} [$r(Y^{3+}) = 0.90$ Å].[32,33] The crystallographic site coordinates, occupancy factors, and equivalent isotropic displacement parameters are summarized in Table 3. The atomic coordinates are quite similar for the doped and undoped $Ba_3Lu_2B_6O_{15}$ compound, while the lattice parameter *a* and the unit cell volume *V* of the doped compound are higher than those of the undoped host lattice due to Eu^{3+} being larger in size than Lu^{3+}.

According to the Rietveld refinement, the overall composition is about $Ba_3Lu_{0.7}Eu_{1.3}B_6O_{15}$, close to the weighed-out

https://doi.org/10.1021/acs.inorgchem.5c03366
Inorg. Chem. 2025, 64, 18588−18598

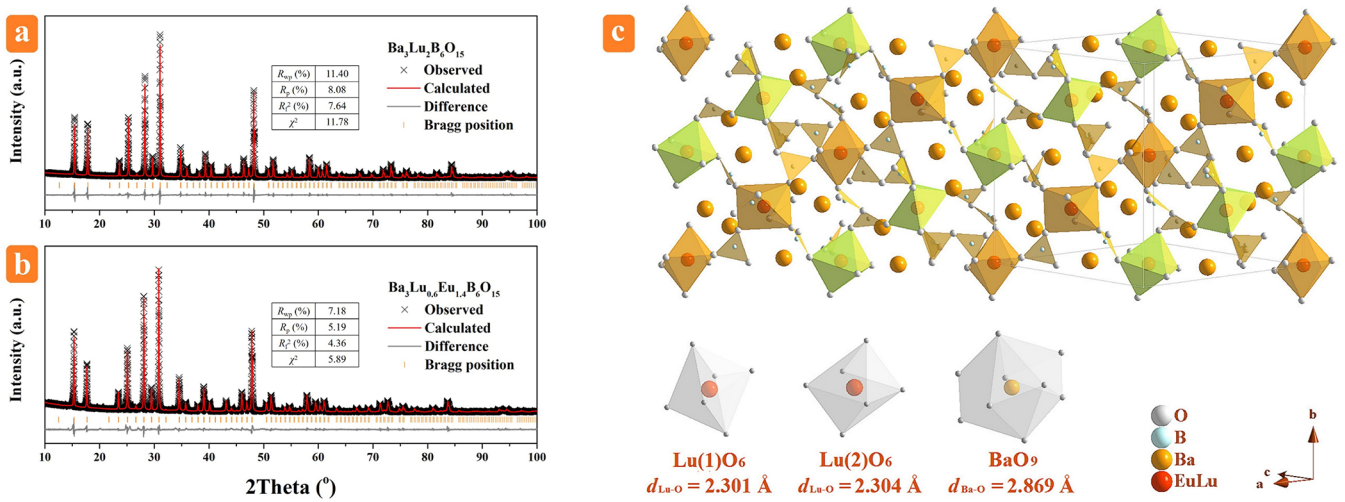

Figure 2. Power XRD patterns of $Ba_3Lu_2B_6O_{15}$ (a) and $Ba_3Lu_{0.6}Eu_{1.4}B_6O_{15}$ (b) with corresponding Rietveld refinement (red) and difference (blue); crystal structure of $Ba_3Lu_{0.6}Eu_{1.4}B_6O_{15}$ (c).

Table 2. Rietveld Refinement Data and Crystallographic Data of $Ba_3Lu_2B_6O_{15}$ and $Ba_3Lu_{0.6}Eu_{1.4}B_6O_{15}$ (Cubic Crystal System with Space Group Ia3̄)

	$Ba_3Lu_2B_6O_{15}$	$Ba_3Lu_{0.6}Eu_{1.4}B_6O_{15}$
a (Å)	14.1550(1)	14.2513(2)
V (Å^3)	2836.17(2)	2894.44(3)
R_{wp} (%)	11.40	7.18
R_p (%)	8.08	5.19
R_f^2 (%)	7.64	4.36
χ^2	11.78	5.89

$Ba_3Lu_{0.6}Eu_{1.4}B_6O_{15}$ composition. For further understanding of the crystal structure of the studied phosphor, a fragment of $Ba_3Lu_{0.6}Eu_{1.4}B_6O_{15}$ unit cell is illustrated in Figure 2c. Clearly, the structure consists of BaO_9 polyhedra and two types of isolated LuO_6 octahedra connected by corner-shared $[B_2O_5]^{4-}$ groups.[33] Atoms Lu1 and Lu2 occupy alternatively the 8a and 8b sites with inversion symmetry (point group C_{3i}) running along the [111] direction. The occupancy of Eu^{3+} on the Lu(1) site seems to be somewhat higher than on the Lu(2) site (Table 2), which is also indicated by the results reported by Kolesnikov et al.[31] This preferential occupation is ascribed to the octahedral site being larger for Lu(1) (15.122 Å^3) as compared to Lu(2) (14.151 Å^3) and may be the reason for some deviation from Vegard's law, as noticed in this work and in the literature.[31] It is interesting to note that such a deviation from Vegard's law was not observed for $Ba_3(Y,Eu)_2B_6O_{15}$ with varying Eu concentrations,[30] probably related to the fact that the size difference between Y^{3+} and Eu^{3+} is less than that between Lu^{3+} and Eu^{3+}.

TEM analysis of a $Ba_3Lu_{0.6}Eu_{1.4}B_6O_{15}$ particle reveals crystalline domains (a1 and a2) with periodic atomic arrangements and preserved long-range order (Figure 3a), showing no observable lattice defects or structural irregularities. EDS mapping confirms the spatial homogeneity of constituent elements (Ba, Lu, Eu, B, and O) across the phosphor particle, with no evidence of localized enrichment or phase separation (Figure 3b and c).

The PLE spectra of $Ba_3Lu_{1.92}Eu_{0.08}B_6O_{15}$ and $Ba_3Lu_{0.6}Eu_{1.4}B_6O_{15}$ are presented in Figure 4a and c. For 595 nm monitoring, the PLE spectra consist of a broad band from 200 to 350 nm, which is ascribed to the charge transfer band (CTB), i.e., the transition of 2p electrons of O^{2-} to the 4f orbitals of Eu^{3+} ($O^{2-} \rightarrow Eu^{3+}$), and various sharp peaks from 300 to 500 nm corresponding to the f−f transitions of Eu^{3+} within its $4f^6$ configuration. The excitation peak located at 398 nm matches well with the emission wavelength of n-UV chips. With the increasing concentration of Eu^{3+} from 4 mol % to 70 mol %, the intensity of excitation peaks becomes stronger as a consequence of a higher absorption of excitation radiation; however, the ratio of the CTB intensity to the 4f−4f transition intensity (CTB/4f−4f) decreases because the lowered local

Table 3. Atomic Coordinates (x, y, z), Site Occupancy, and Isotropic Displacement Parameters (U_{iso}) of $Ba_3Lu_2B_6O_{15}$ and $Ba_3Lu_{0.6}Eu_{1.4}B_6O_{15}$

	$Ba_3Lu_2B_6O_{15}$					$Ba_3Lu_{0.6}Eu_{1.4}B_6O_{15}$				
Site	x	y	z	$Occ.$	U_{iso}	x	y	z	$Occ.$	U_{iso}
Ba1	0.3678(5)	0	0.25	1	0.0244(15)	0.3671(5)	0	0.25	1	0.0302(18)
Lu1	0	0	0	1	0.0331(17)	0	0	0	0.3009(12)	0.0361(29)
Lu2	0.25	0.25	0.25	1	0.0228(21)	0.25	0.25	0.25	0.4227(15)	0.0244(24)
Eu1	-	-	-	-	-	0	0	0	0.6991(12)	0.0361(31)
Eu2	-	-	-	-	-	0.25	0.25	0.25	0.5773(15)	0.0244(25)
B1	0.0596(7)	0.3073(6)	0.1207(7)	1	0.0364(25)	0.0713(8)	0.2979(6)	0.1145(6)	1	0.0138(18)
O1	0.0325(5)	0.0385(7)	0.3467(8)	1	0.0249(20)	0.0300(8)	0.0375(5)	0.3456(5)	1	0.0479(42)
O2	0.1619(6)	0	0.25	1	0.0368(30)	0.1595(7)	0	0.25	1	0.0254(33)
O3	0.1431(7)	0.3218(7)	0.1551(8)	1	0.0254(19)	0.1412(5)	0.3252(8)	0.1574(7)	1	0.0113(14)

https://doi.org/10.1021/acs.inorgchem.5c03366
Inorg. Chem. 2025, 64, 18588−18598

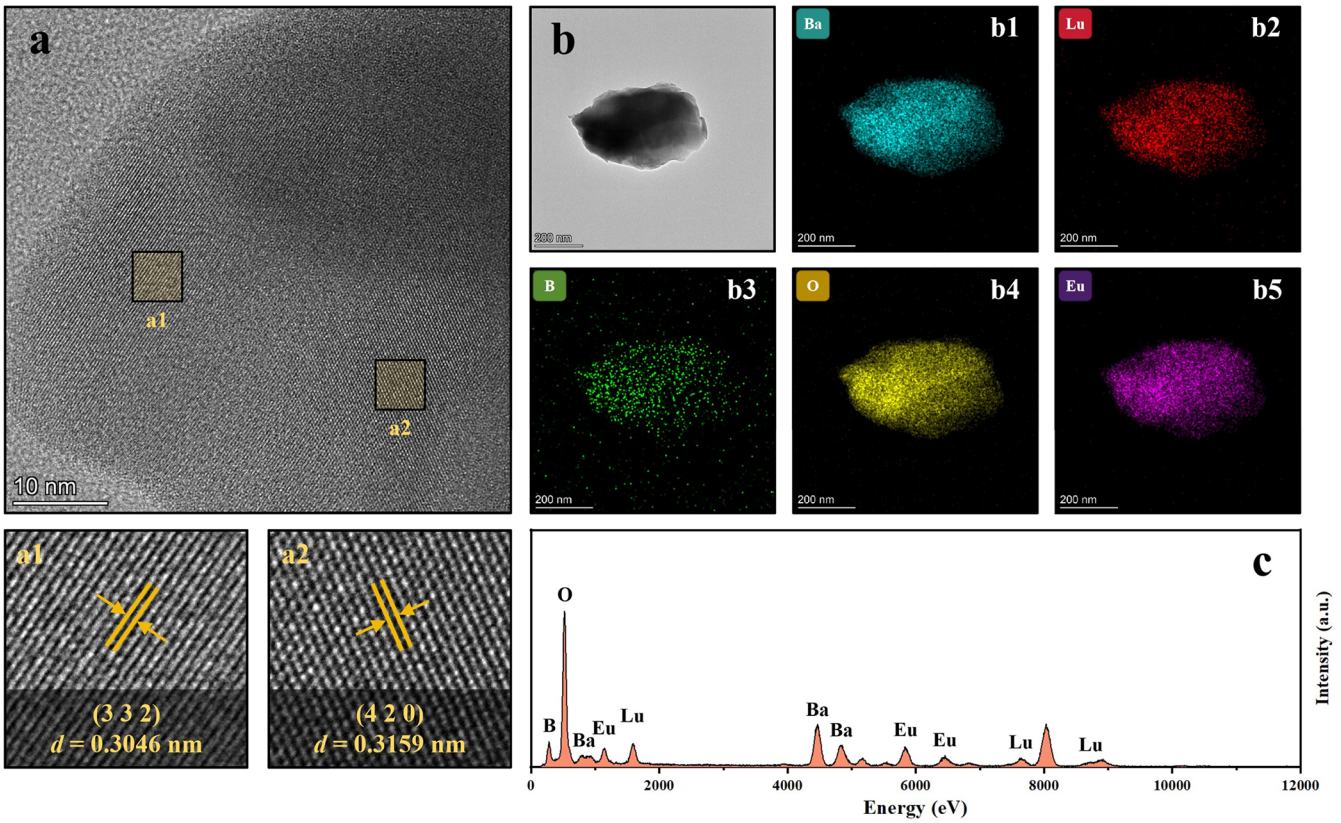

Figure 3. High-resolution TEM (a), elemental mappings (b), and EDS (c) of a $Ba_3Lu_{0.6}Eu_{1.4}B_6O_{15}$ particle.

symmetry around Eu^{3+} sites selectively enhances the parity-forbidden 4f−4f transitions more than the parity-allowed CTB. At the same time, the CTB of $Ba_3Lu_{0.6}Eu_{1.4}B_6O_{15}$ shifts to a longer wavelength (i.e., lower energy) compared to that of $Ba_3Lu_{1.92}Eu_{0.08}B_6O_{15}$, which is attributed to the longer Eu−O distance and the higher bond covalency as a consequence of the substitution of Lu^{3+} by Eu^{3+}.[34]

For the PL spectrum of $Ba_3Lu_{1.92}Eu_{0.08}B_6O_{15}$ with an excitation wavelength of 398 nm, line emissions typical for Eu^{3+} are observed, peaking at 582, 595, 614, 655, and 707 nm (Figure 4b), which are attributed to 4f−4f transitions $^5D_0 \rightarrow {}^7F_J$ (J = 0, 1, 2, 3, 4) of Eu^{3+}. It is known that the magnetic dipole transition ($^5D_0 \rightarrow {}^7F_1$) of Eu^{3+} will be dominant if Eu^{3+} ions are located at inversion-symmetrical sites, whereas the electric dipole transition ($^5D_0 \rightarrow {}^7F_2$) will be dominant in the absence of inversion symmetry.[35] Normally, for most Eu^{3+}-activated phosphors, the red emission due to the $^5D_0 \rightarrow {}^7F_2$ transition (at about 615 nm) is the strongest, but for $Ba_3Lu_2B_6O_{15}$:Eu^{3+}, the orange emission due to the $^5D_0 \rightarrow {}^7F_1$ transitions (in the range 585−600 nm) is the strongest. This indicates that Eu^{3+} is substituted on Lu^{3+} sites with inversion symmetry,[36] in agreement with the crystal structure (i.e., 8a and 8b sites in $Ba_3Lu_2B_6O_{15}$ with C_{3i} point symmetry), and the magnetic dipole transition is the primary transition in this luminescence process. A similar dominant $^5D_0 \rightarrow {}^7F_1$ transition for Eu^{3+} has been reported previously in several other reddish-orange-emitting phosphors with inversion-symmetric Ln sites, such as $InBO_3$:Eu^{3+} (O/R = 4.2, with C_{3i} point symmetry of In),[37] $Y_2Sn_2O_7$:Eu^{3+} (O/R = 7.1, with D_{3d} point symmetry of Y),[38] and Ba_2MgWO_6:Eu^{3+} (O/R = 10.0, with O_h point symmetry of Mg).[39]

For Eu^{3+} located on a site with C_{3i} inversion center, a splitting of the $^5D_0 \rightarrow {}^7F_1$ transition into 2 lines is expected.[17] Assuming that the 582 nm emission line can be attributed to the $^5D_0 \rightarrow {}^7F_0$ transition, only two $^5D_0 \rightarrow {}^7F_1$ emission lines are observed, while for two Eu^{3+} centers (Eu on Lu1 and Lu2 sites), actually 2 × 2 = 4 lines are expected. This indicates that the two Eu^{3+} centers resemble each other very much, in agreement with the very similar coordination of the two octahedral Lu^{3+} sites with both inversion symmetry. As normally, the $^5D_0 \rightarrow {}^7F_3$ transition (at about 655 nm) is weak, but for $Ba_3Lu_2B_6O_{15}$:Eu^{3+} also, the $^5D_0 \rightarrow {}^7F_4$ emission (at about 705 nm) is weak, indicating long-range order.[33] The relatively weak $^5D_0 \rightarrow {}^7F_4$ transition is beneficial for high lumen efficiency because 707 nm is outside the eye sensitivity curve.[40] The PL spectrum of $Ba_3Lu_{0.6}Eu_{1.4}B_6O_{15}$ (Figure 4d) shows a similar shape but much higher intensity than that of $Ba_3Lu_{1.92}Eu_{0.08}B_6O_{15}$ as a consequence of the higher Eu concentration.

In order to describe the emission color of $Ba_3Lu_{0.6}Eu_{1.4}B_6O_{15}$ more clearly from an application point of view, the CIE chromaticity diagram with the $Ba_3Lu_{0.6}Eu_{1.4}B_6O_{15}$ phosphor and the photograph of its emission upon excitation with 365 nm are presented in Figure 4e, showing a bright reddish-orange emission. The color coordinates of the $Ba_3Lu_{0.6}Eu_{1.4}B_6O_{15}$ phosphor are calculated to be (x = 0.605, y = 0.387) in the orange region of the CIE chromaticity diagram, which is quite similar to what is reported for $Ba_3Y_{1.3}Eu_{0.7}B_6O_{15}$ (x = 0.601, y = 0.396).[30] On the basis of the standard of NTSC and the European Broadcasting Union (EBU), the color purity, as another important factor for monochromatic light, has been calculated according to the following equation:[41]

https://doi.org/10.1021/acs.inorgchem.5c03366
Inorg. Chem. 2025, 64, 18588−18598

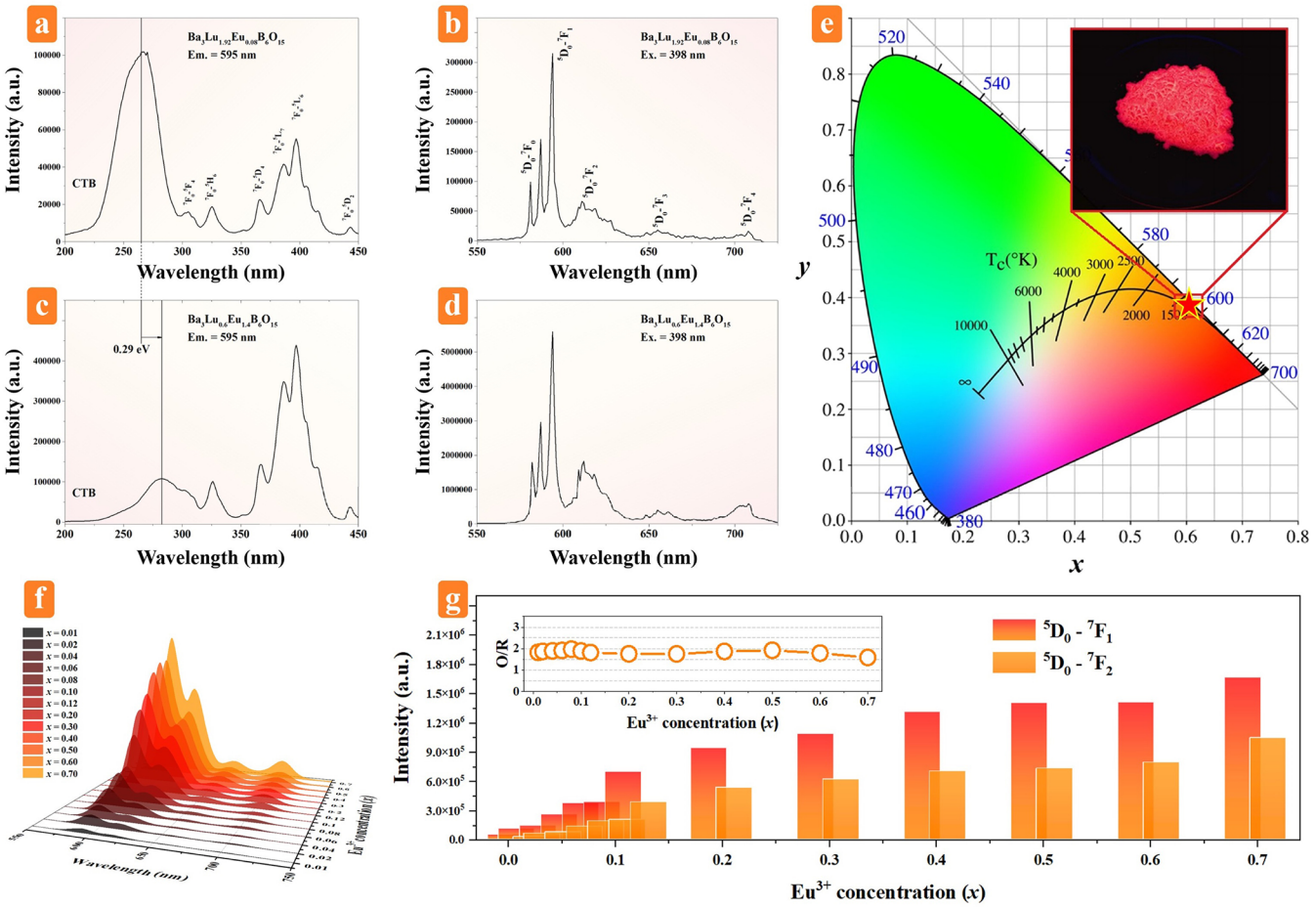

Figure 4. PLE spectra of $Ba_3Lu_{1.92}Eu_{0.08}B_6O_{15}$ (a) and $Ba_3Lu_{0.6}Eu_{1.4}B_6O_{15}$ (c); PL spectra of $Ba_3Lu_{1.92}Eu_{0.08}B_6O_{15}$ (b) and $Ba_3Lu_{0.6}Eu_{1.4}B_6O_{15}$ (d); CIE chromaticity diagram and photograph of $Ba_3Lu_{0.6}Eu_{1.4}B_6O_{15}$ upon excitation with 365 nm (e); PL spectra of $Ba_3Lu_{2(1-x)}Eu_{2x}B_6O_{15}$ depending on the Eu^{3+} doping concentration (f); the emission intensities of $^5D_0 \rightarrow {}^7F_1$ and $^5D_0 \rightarrow {}^7F_2$ transitions and orange (O)/red (R) intensity ratio as a function of the Eu^{3+} concentration (g).

$$\text{Color purity} = \frac{\sqrt{(x - x_i)^2 + (y - y_i)^2}}{\sqrt{(x_d - x_i)^2 + (y_d - y_i)^2}} \times 100\% \quad (2)$$

where (x, y), (x_i, y_i), and (x_d, y_d) stand for the CIE chromaticity coordinates of the studied $Ba_3Lu_{0.6}Eu_{1.4}B_6O_{15}$ phosphor (0.605, 0.387), white illumination (0.333, 0.333), and dominant emission wavelength (0.612, 0.388), respectively. The calculation demonstrates that the color purity can be as high as 97.5%, which is close to that of other Eu^{3+}-activated reddish-orange-emitting phosphors, such as $KBaBP_2O_8:Eu^{3+}$ (98.7%).[42] It indicates that the emission color of $Ba_3Lu_{0.6}Eu_{1.4}B_6O_{15}$ is extremely close to the spectral edge of the 1931 CIE chromaticity diagram due to the dominant $^5D_0 \rightarrow {}^7F_1$ line transition of Eu^{3+}.

The PL spectra of $Ba_3Lu_{2(1-x)}Eu_{2x}B_6O_{15}$ under excitation at 398 nm depending on the Eu^{3+} doping concentration are presented in Figure 4f. All the peaks exhibit a similar shape and position relative to each other. As can be seen from Figure 4f and g, the emission intensity of $Ba_3Lu_2B_6O_{15}:Eu^{3+}$ enhances progressively with the increasing concentration of Eu^{3+} ions, while the ratio between $^5D_0 \rightarrow {}^7F_1$ and $^5D_0 \rightarrow {}^7F_2$ emissions remains nearly constant, with a value significantly higher than 1. This means that the inversion-symmetric coordination of Eu^{3+} remains preserved at higher Eu concentrations despite reaching the maximum solubility of Eu in $Ba_3Lu_2B_6O_{15}$ at about 900 °C. In addition, it has to be noted that no decrease in emission intensity has been observed within the experimental doping range of Eu^{3+} ions. Such a high doping concentration of Eu^{3+} in $Ba_3Lu_2B_6O_{15}$ without concentration quenching is considerably higher than that of most other reported Eu^{3+}-activated phosphors in general.

Actually, the concentration quenching behavior cannot be judged simply from the emission intensity, which not only depends on the quantum efficiency but also on the absorption of excitation radiation, which will increase with higher Eu concentrations.[43] Therefore, the IQE of $Ba_3Lu_{2(1-x)}Eu_{2x}B_6O_{15}$ was determined, and the IQE values of $Ba_3Lu_{2(1-x)}Eu_{2x}B_6O_{15}$ increase from 17% ($x = 0.04$) to 53% ($x = 0.7$) upon excitation with 398 nm (Figure S1), which is much higher than the maximum quantum yield reported for $Ba_3Lu_2B_6O_{15}$:Eu in the literature.[31] The difference can be explained by a higher phase purity of our samples and indicates that further improvement may be anticipated by the optimization of synthesis conditions. The maximum IQE value of $Ba_3Lu_2B_6O_{15}$:Eu is also higher than that obtained for $Ba_3Y_2B_6O_{15}:Eu^{3+}$ (about 13%),[30] in line with trends that the quantum efficiency of Eu^{3+}-activated phosphors gets larger for smaller Ln^{3+} on which Eu^{3+} is incorporated ($La^{3+} < Y^{3+} < Lu^{3+}$).[44]

https://doi.org/10.1021/acs.inorgchem.5c03366
Inorg. Chem. 2025, 64, 18588−18598

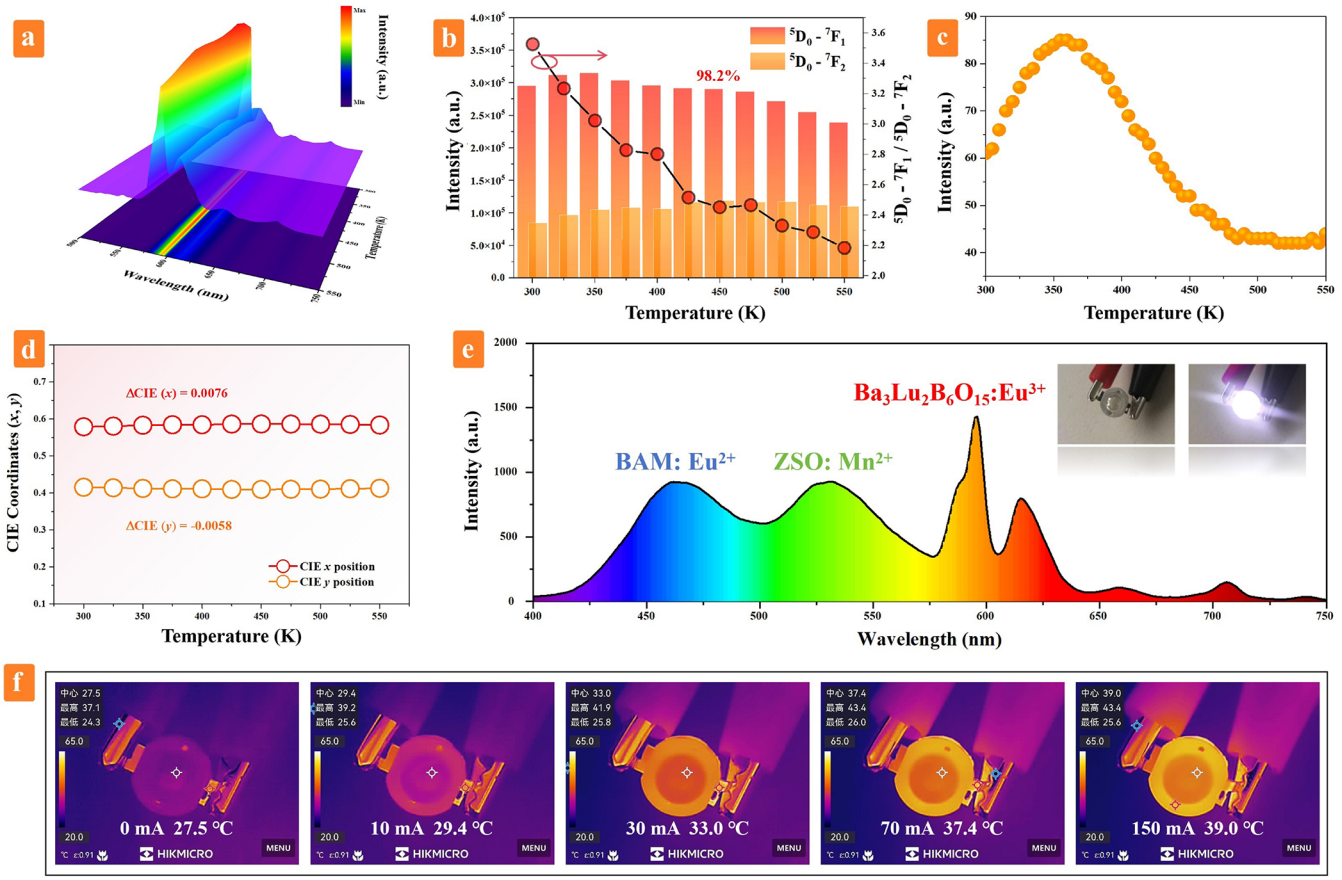

Figure 5. Temperature-dependent PL spectra of $Ba_3Lu_{0.8}Eu_{1.2}B_6O_{15}$ (a); emission intensities of $^5D_0 \rightarrow {}^7F_1$ and $^5D_0 \rightarrow {}^7F_2$ transitions (b), TL glow curves of $Ba_3Lu_{0.8}Eu_{1.2}B_6O_{15}$ (c), and CIE chromaticity coordinates as a function of temperature (d); spectra and photographs of the (on/off) LED device fabricated using a mixture of $Ba_3Lu_{0.8}Eu_{1.2}B_6O_{15}$, $BaMgAl_{10}O_{17}$:Eu^{2+} (BAM:Eu^{2+}), and Zn_2SiO_4:Mn^{2+} (ZSO:Mn^{2+}) phosphors (e); thermal imaging results of the LED under various driving currents (0, 10, 30, 70, and 150 mA) (f).

Furthermore, the increasing IQE value indicates the nonexistent concentration quenching, at least until 70 mol % of Eu^{3+} in $Ba_3Lu_2B_6O_{15}$. The lower quenching concentration (about 18 mol % Eu) reported for $Ba_3Lu_2B_6O_{15}$:Eu in the literature[31] is related to the presence of secondary phases and consequently, a higher concentration of defects. Also, for $Ba_3Y_2B_6O_{15}$:Eu, a high quenching concentration of about 35 mol % Eu has been found.[30]

To explain the high quenching concentration of Eu^{3+} emission in $Ba_3Ln_2B_6O_{15}$ (Ln = Lu, Y) host lattices, we have to consider the $Ba_3Ln_2B_6O_{15}$ structure. As we mentioned, the Eu^{3+} ions are surrounded by six O^{2-} anions in a symmetric octahedral configuration, while each O^{2-} anion is connected to a $[B_2O_5]^{4-}$ group. Thus, the Eu^{3+} ions are spaced completely apart from each other without sharing any O^{2-} ions. Moreover, the Ln^{3+} coordination octahedrons, connected by $[B_2O_5]^{-}$ groups, form an isolated chain structure along the [111] direction (Figure 2). This chain-like structure is equally applicable to both Ln(1) and Ln(2), so the interactions between the Eu^{3+} ions are largely present in one dimension. Indeed, the intrachain distance between two nearest Lu^{3+} ions in $Ba_3Lu_2B_6O_{15}$, with a value of approximately 6.17 Å, is shorter than the interchain distance of about 7.13 Å[31] Therefore, the nonradiative energy migrations in $Ba_3Lu_2B_6O_{15}$:Eu predominately take place inside the Lu^{3+}/Eu^{3+} chains, followed by energy transfer to the nearby quenching sites, which results in less chance for migrating excitation energy to reach the randomly distributed quenching sites.[45−48]

The critical distance (R_c) for nonradiative energy transfer among Eu^{3+} ions can be calculated by estimating the average distance between two adjacent Eu^{3+} ions according to the following equation by Blasse:[44]

$$R_c \approx 2\left(\frac{3V}{4\pi x_c N}\right)^{1/3} \tag{3}$$

where V is the volume of the unit cell, x_c is the critical concentration of activator ion Eu^{3+}, and N is the number of Lu ions per unit cell. Because of the strong resemblance in the coordination of Lu(1) and Lu(2), we do not discriminate between the various options of energy transfer (Eu(1) → Eu(1), Eu(2) → Eu(2), Eu(1) → Eu(2) and Eu(2) → Eu(1)). Using input values of V = 2894 Å^3, N = 16, and x_c larger than 0.7, the calculated value of R_c is less than about 7.9 Å, which is smaller than that reported by Annadurai et al. for Eu^{3+} in $Ba_3Y_2B_6O_{15}$ (i.e., 9.98 Å for x_c = 0.35 with $0 < x < 1$).[30] It should be noted that the R_c calculated in this way generally represents the average distance among activator ions in the host lattice, but in this case, the average distance between Eu^{3+} ions along the 1D chain direction ([111]) is shorter than that along other directions. A guess can be made by taking the Lu−Lu intrachain distance of 6.17 Å divided by 0.7 (70% of Lu replaced by Eu), resulting in an average distance of about 8.8

https://doi.org/10.1021/acs.inorgchem.5c03366
Inorg. Chem. 2025, 64, 18588−18598

Å. Considering the critical distances being in the range of 8−10 Å, it can be speculated that also exchange interaction (critical distance below 10 Å)[48] between Eu^{3+} ions in the one-dimensional chains may contribute to some minor extent to concentration quenching, in addition to the dominant effect of electric multipole−multipole interactions (critical distance above 15 Å)[48] between Eu^{3+} ions in different one-dimensional chains.

The fluorescence decay curves of Eu^{3+} emission at 594 nm in $Ba_3Lu_2B_6O_{15}:Eu^{3+}$ excited at 365 nm are shown in Figure S2. The lifetime τ can be calculated according to the following nonexponential equation:[49]

$$\tau = \frac{\int_0^\infty I(t)t\ \mathrm{d}t}{\int_0^\infty I(t)\ \mathrm{d}t} \tag{4}$$

In the equation above, $I(t)$ means the emission intensity at time t. The fluorescent lifetimes of Eu^{3+} at 594 nm are determined to be 4.11, 4.16, 4.17, 4.19, 4.10, 4.11, 4.07, 4.14, 4.10, 4.14, 4.15, 4.15, and 4.10 ms for the doping concentrations from 1 mol % to 70 mol %, respectively. The decay time is higher as compared to other Eu^{3+}-doped phosphors with the $^5D_0 \rightarrow {}^7F_2$ transition as the dominant emission, with typical values of around 1 ms. This is related to the fact that the electric-dipole transition is forbidden for $Ba_3Ln_2B_6O_{15}$ (Ln = Lu, Y) host lattices with inversion symmetry at the Ln site. For other phosphors with centrosymmetric Eu^{3+} coordination, resulting in the magnetic dipole $^5D_0 \rightarrow {}^7F_1$ emission being dominant, decay times larger than 5 ms have been reported (e.g., 5.71 ms for $Ba_2MgWO_6:Eu^{3+}$ with O_h symmetry,[50] 7.4 ms for $InBO_3:Eu^{3+}$ with S6 (C_{3i}) symmetry,[51] 6.34 ms for $ScBO_3:Eu^{3+}$ with S_6 (C_{3i}) symmetry[52]). The clear difference between the magnitude of the decay time for Eu^{3+} on a site with versus without inversion symmetry is well illustrated by $Y_2O_3:Eu^{3+}$ for which a decay time of 0.96−1.76 ms has been measured for the C_2 site (without inversion symmetry) and 5.5−7.9 ms for the S_6 (C_{3i}) site (with inversion symmetry).[53] In addition, the decay lifetime of the Eu^{3+} ions does not decrease with increasing Eu^{3+} concentration, which further proves that there is no concentration quenching in the as-studied phosphors.

Thermal quenching behavior, as another important phosphor characteristic, needs also to be taken into consideration for the assessment of the phosphor for *w*-LED applications. The temperature-dependent PL spectra of $Ba_3Lu_{0.8}Eu_{1.2}B_6O_{15}$ under excitation at 398 nm are shown in Figure 5a, and the emission intensities of $^5D_0 \rightarrow {}^7F_1$ and $^5D_0 \rightarrow {}^7F_2$ transitions are illustrated in Figure 5b. A small increase (6.6% at maximum) of the emission intensity can be observed when increasing the temperature from 300 to 350 K, which may be ascribed to the emptying of thermally activated traps that store and transfer energy to $^5D_0$ energy levels of Eu^{3+}.[54,55] To demonstrate the anomalous thermal quenching behavior of the phosphor, Figure 5c presents the TL spectrum. As the temperature approaches 350 K, the carriers trapped in defect states are gradually released due to increased thermal energy, followed by participation in the radiative transitions of the Eu^{3+} excited states. At this stage, a dynamic balance is achieved between the intensity increase as a consequence of trap release and the intensity decrease due to nonradiative losses, leading to the emission intensity reaching a maximum value. When the temperature exceeds 350 K, intensified lattice vibrations enhance multiphonon relaxation or radiationless crossover takes place via the Eu^{3+} charge transfer band, causing the energy of the Eu^{3+} excited states to dissipate via nonradiative pathways. Concurrently, the trapped carriers will have become depleted, significantly suppressing radiative recombination efficiency and resulting in a decline in luminescence intensity. Notably, the emission intensity decreases only slightly at higher temperatures and retains about 98% at 450 K compared with that at room temperature. This is much better than that reported for other Eu^{3+}-activated phosphors, such as $Ca_3Gd(AlO)_3(BO_3)_4:Eu^{3+}$ (84% at 423 K, λ_{ex} = 397 nm),[56] $Na_2Y_2B_2O_7:Eu^{3+}$ (40.2% at 423 K, λ_{ex} = 395 nm),[57] $Ba_2Gd_5B_5O_{17}:Eu^{3+}$ (73.8% at 423 K, λ_{ex} = 396 nm),[58] and $Ba_3Y_2B_6O_{15}:Eu^{3+}$ (53.1% at 423 K, λ_{ex} = 393 nm),[30] implying that the $Ba_3Lu_{0.8}Eu_{1.2}B_6O_{15}$ phosphor shows superior thermal stability.

Furthermore, we studied the chromaticity stability during an increase of temperature (Figure 5d). With increasing temperature, the $^5D_0 \rightarrow {}^7F_1$ emission intensity decreases, while the $^5D_0 \rightarrow {}^7F_2$ emission intensity somewhat increases (Figure 5b). So, the $^5D_0 \rightarrow {}^7F_1/{}^5D_0 \rightarrow {}^7F_2$ ratio decreases at higher temperatures, indicating that the local coordination of the Eu^{3+} center deviates from exact inversion symmetry, probably due to enhanced vibrations.[30,59] However, the values of chromaticity coordinates x and y change only within a small range, and the phosphor presents a very limited color shift as a function of the sample temperature (Figure 5d). It indicates that the studied phosphor has excellent thermal and chromaticity stability and shows promising application prospects in the fields of lighting and display devices.

Given its promising luminescence properties, we further constructed a white LED device using $Ba_3Lu_{0.8}Eu_{1.2}B_6O_{15}$ as the reddish-orange-emitting component. Specifically, the phosphor was blended with a 365 nm UV chip, along with the commercial blue-emitting phosphor $BaMgAl_{10}O_{17}:Eu^{2+}$ ($BAM:Eu^{2+}$) and the green-emitting phosphor $Zn_2SiO_4:Mn^{2+}$ ($ZSO:Mn^{2+}$), in a mass ratio of 6:1.5:1 (Figure 5e). Under a 150 mA driving current, the LED emits bright white light with CIE (0.31, 0.35) and R_a = 85, without additional color-balancing filters while maintaining a low operating temperature (39.0 °C) (Figure 5f). This confirms the phosphor's potential as a reddish-orange emitter in *w*-LEDs.

4. CONCLUSIONS

Eu^{3+}-doped $Ba_3Lu_2B_6O_{15}$ phosphors with varying Eu contents were synthesized in air via a multistep high-temperature solid-state reaction. The maximum solubility of Eu^{3+} replacing Lu^{3+} in the $Ba_3Lu_2B_6O_{15}$ host lattice synthesized at 910 °C is between 70 and 80 mol %. All studied Eu^{3+}-doped $Ba_3Lu_2B_6O_{15}$ phosphors show intense reddish-orange emission with a long decay time (about 4.1 ms) upon excitation at 398 nm, originating from the magnetic dipole $^5D_0 \rightarrow {}^7F_1$ transition of Eu^{3+} ions occupying Lu^{3+} sites with inversion symmetry (C_{3i} point group). Notably, no obvious concentration quenching was observed up to 70 mol % Eu, ascribed to the unique one-dimensional lattice structure, limiting efficient energy migration to the Lu−Lu chains. The $Ba_3Lu_{0.8}Eu_{1.2}B_6O_{15}$ composition demonstrated exceptional thermal stability, retaining ∼98% of its room-temperature emission intensity at 450 K, with a minimal chromaticity shift (ΔCIE < 0.01) across the temperature range. The best, not yet optimized, $Ba_3Lu_{0.6}Eu_{1.4}B_6O_{15}$ sample achieved a high IQE of ∼53%, accompanied by vivid reddish-orange emission with CIE

https://doi.org/10.1021/acs.inorgchem.5c03366
Inorg. Chem. 2025, 64, 18588−18598

coordinates (0.605, 0.387) and a color purity exceeding 97.5%. When combined with commercial blue-emitting (BAM:Eu^{2+}) and green-emitting (ZSO:Mn^{2+}) phosphors on a 365 nm UV chip, the integrated white LED device delivered bright illumination with CIE coordinates (0.31, 0.35) and an R_a of 85. These findings collectively validate the $Ba_3Lu_2B_6O_{15}$:Eu^{3+} phosphor as a highly promising candidate for high-performance warm white LED applications, particularly benefiting from its combination of excellent thermal stability, superior color purity, and efficient energy utilization.

■ ASSOCIATED CONTENT

Supporting Information

The Supporting Information is available free of charge at https://pubs.acs.org/doi/10.1021/acs.inorgchem.5c03366.

IQE spectra, fluorescence decay curves, and crystallographic data (PDF)

■ AUTHOR INFORMATION

Corresponding Authors

Ziyao Wang − *Key Laboratory of Eco-restoration of Regional Contaminated Environment, Ministry of Education, Shenyang University, Shenyang 110044, China; Group Luminescent Materials, Section Fundamental Aspects of Materials and Energy, Faculty of Applied Sciences, Delft University of Technology, Delft 2629 JB, The Netherlands;* orcid.org/0000-0001-6632-4540; Email: wzy@syu.edu.cn

Yangai Liu − *Beijing Key Laboratory of Materials Utilization of Nonmetallic Minerals and Solid Wastes, National Laboratory of Mineral Materials, School of Materials Science and Technology, China University of Geosciences Beijing, Beijing 100083, China;* orcid.org/0000-0002-8148-1699; Email: liuyang@cugb.edu.cn

H. T. Hintzen − *Group Luminescent Materials, Section Fundamental Aspects of Materials and Energy, Faculty of Applied Sciences, Delft University of Technology, Delft 2629 JB, The Netherlands*; Email: H.T.Hintzen@tudelft.nl

Authors

Shengtao Ren − *Key Laboratory of Eco-restoration of Regional Contaminated Environment, Ministry of Education, Shenyang University, Shenyang 110044, China*

Ximing Kong − *Key Laboratory of Eco-restoration of Regional Contaminated Environment, Ministry of Education, Shenyang University, Shenyang 110044, China*

Mingpan Wei − *Key Laboratory of Eco-restoration of Regional Contaminated Environment, Ministry of Education, Shenyang University, Shenyang 110044, China*

Benjamin Dierre − *Group Luminescent Materials, Section Fundamental Aspects of Materials and Energy, Faculty of Applied Sciences, Delft University of Technology, Delft 2629 JB, The Netherlands*

Ruben Abellon − *Department of Chemical Engineering, Faculty of Applied Sciences, Delft University of Technology, Delft 2629 HZ, The Netherlands*

Complete contact information is available at: https://pubs.acs.org/10.1021/acs.inorgchem.5c03366

Author Contributions

The manuscript was written through contributions of all authors. All authors have given approval to the final version of the manuscript.

Notes

The authors declare no competing financial interest.

■ ACKNOWLEDGMENTS

This work was supported by the Research Foundation of Education Department of Liaoning Province (Grant No. JYTQN2023280).

■ REFERENCES

(1) Li, G.; Tian, Y.; Zhao, Y.; Lin, J. Recent progress in luminescence tuning of Ce^{3+} and Eu^{2+}-activated phosphors for pc-WLEDs. *Chem. Soc. Rev.* **2015**, *44*, 8688−8713.

(2) Pust, P.; Schmidt, P. J.; Schnick, W. A revolution in lighting. *Nat. Mater.* **2015**, *14*, 454−458.

(3) Shang, M.; Li, C.; Lin, J. How to produce white light in a single-phase host? *Chem. Soc. Rev.* **2014**, *43*, 1372−1386.

(4) Lin, C. C.; Liu, R. S. Advances in phosphors for light-emitting diodes. *J. Phys. Chem. Lett.* **2011**, *2*, 1268−1277.

(5) Li, J.; Yan, J.; Wen, D.; Khan, W. U.; Shi, J.; Wu, M.; Su, Q.; Tanner, P. A. Advanced red phosphors for white light-emitting diodes. *J. Mater. Chem. C* **2016**, *4*, 8611−8623.

(6) Oh, J. H.; Eo, Y. J.; Yoon, H. C.; Huh, Y.; Do, Y. R. Evaluation of new color metrics: Guidelines for developing narrow-band red phosphors for WLEDs. *J. Mater. Chem. C* **2016**, *4*, 8326−8348.

(7) Guo, C.; Huang, D.; Su, Q. Methods to improve the fluorescence intensity of CaS: Eu^{2+} red-emitting phosphor for white LED. *Mater. Sci. Eng.* **2006**, *130*, 189−193.

(8) Li, Y. Q.; de With, G.; Hintzen, H. T. The effect of replacement of Sr by Ca on the structural and luminescence properties of the red-emitting $Sr_2Si_5N_8$: Eu^{2+} LED conversion phosphor. *J. Solid State Chem.* **2008**, *181* (3), 515−524.

(9) Lei, B.; Machida, K.; Horikawa, T.; Hanzawa, H. Synthesis and photoluminescence properties of $CaAlSiN_3$: Eu^{2+} nanocrystals. *Chem. Lett.* **2010**, *39*, 104−105.

(10) Sijbom, H. F.; Verstraete, R.; Joos, J. J.; Poelman, D.; Smet, P. F. K_2SiF_6: Mn^{4+} as a red phosphor for displays and warm-white LEDs: A review of properties and perspectives. *Opt. Mater. Express* **2017**, *7* (9), 3332−3365.

(11) Oh, J. H.; Kang, H.; Eo, Y. J.; Park, H. K.; Do, Y. R. Synthesis of narrow-band red-emitting K_2SiF_6: Mn^{4+} phosphors for a deep red monochromatic LED and ultrahigh color quality warm-white LEDs. *J. Mater. Chem. C* **2015**, *3*, 607−615.

(12) Ye, S.; Xiao, F.; Pan, Y. X.; Ma, Y. Y.; Zhang, Q. Y. Phosphors in phosphor-converted white light-emitting diodes: Recent advances in materials, techniques and properties. *Mater. Sci. Eng., R* **2010**, *71*, 1−34.

(13) Sohn, K. S.; Park, D. H.; Cho, S. H.; Kwak, J. S.; Kim, J. S. Computational evolutionary optimization of red phosphor for use in tricolor white LEDs. *Chem. Mater.* **2006**, *18*, 1768−1772.

(14) Kanehisa, O.; Kano, T.; Yamamoto, H. Formation process of Y_2O_2S: Eu^{3+} in a preparation with flux. *J. Electrochem. Soc.* **1985**, *132*, 2023.

(15) Fengyang, Z.; Yanpeng, L.; Guangzhou, Z.; Xianqing, P.; Zhuo, S. Orange-red emitting Eu^{2+}-activated $(Sr_{0.883}Ba_{0.1}Lu_{0.017})_3(Si_{0.95}Al_{0.05})O_5$ phosphor: Structure, photoluminescence, and application in white LEDs. *J. Rare Earths* **2015**, *33* (5), 469−474.

(16) Liu, Q.; Xiang, Q.; Song, Z.; Cui, D.; Xia, Z. The synthesis of narrow-band red-emitting $SrLiAl_3N_4$: Eu^{2+} phosphor and improvement of its luminescence properties. *J. Mater. Chem. C* **2016**, *4*, 7332−7338.

(17) Binnemans, K. Interpretation of europium(III) spectra. *Coordin Chem. Rev.* **2015**, *295*, 1−45.

(18) Kumar, D.; Sharma, M.; Pandey, O. P. Morphology controlled Y_2O_3: Eu^{3+} nanophosphors with enhanced photoluminescence properties. *J. Lumin.* **2015**, *158*, 268−274.

(19) Antic, Z.; Krsmanovic, R.; Dordevic, V.; Dramicanin, T.; Dramicanin, M. D. Optical properties of Y_2O_3: Eu^{3+} red emitting

phosphor obtained via spray pyrolysis. *Acta Phys. Pol. A* **2009**, *116*, 622−624.
(20) Raja, D. S.; Lin, P.-C.; Liu, W.-R.; Zhan, J.-X.; Fu, X.-Y.; Lin, C.-H. Multidimensional (0D to 3D) alkaline-earth metal diphosphonates: Synthesis, structural diversity, and luminescence properties. *Inorg. Chem.* **2015**, *54*, 4268−4278.
(21) Yadav, R.; Khan, A. F.; Yadav, A.; Chander, H.; Haranath, D.; Gupta, B. K.; Shanker, V.; Chawla, S. Intense red-emitting $Y_4Al_2O_9$: Eu^{3+} phosphor with short decay time and high color purity for advanced plasma display panel. *Opt. Express* **2009**, *17*, 22023−22030.
(22) Chang, Y. S.; Huang, F. M.; Chen, H. L.; Tsai, Y. Y. Effects of Na_2CO_3 flux addition on the structure and photoluminescence properties for Eu^{3+}-doped YVO_4 phosphor. *J. Phys. Chem. Solids* **2011**, *72*, 1117−1121.
(23) Folkerts, H. F.; Blasse, G. Luminescence of Pb in several calcium borates. *J. Mater. Chem.* **1995**, *5*, 273−276.
(24) Shahare, D. I.; Dhoble, S. J.; Moharil, S. V. Preparation and characterization of magnesium-borate phosphor. *J. Mater. Sci. Lett.* **1993**, *12*, 1873−1874.
(25) Lin, C.; Yu, M.; Pang, M.; Lin, J. Preparation and luminescent properties of $GdMgB_5O_{10}$ doped with Ce^{3+} or/and Tb^{3+} by sol-gel method. *J. Rare Earth* **2005**, *23*, 266−270.
(26) Xu, H.; Zhuang, W.; Wen, X.; Liu, R.; Hu, Y.; Xia, T. Effect of Li^+ ions doping on structure and luminescence of $(Y,Gd)BO_3$: Tb^{3+}. *J. Rare Earths* **2010**, *28* (5), 701−704.
(27) Chaminade, J. P.; Garcia, A.; Pouchard, M.; Fouassier, C.; Jacquier, B.; Perret-Gallix, D.; Gonzalez-Mestres, L. Crystal growth and characterization of $InBO_3$: Tb^{3+}. *J. Cryst. Growth* **1990**, *99*, 799−804.
(28) Li, B.; Annadurai, G.; Sun, L.; Liang, J.; Wang, S.; Sun, Q.; Huang, X. High-efficiency cubic-phased blue-emitting $Ba_3Lu_2B_6O_{15}$: Ce^{3+} phosphors for ultraviolet-excited white-light-emitting diodes. *Opt. Lett.* **2018**, *43*, 5138−5141.
(29) Huang, X.; Guo, H.; Sun, L.; Sakthivel, T.; Wu, Y. A high-efficiency, broadband-excited cyan-emitting $Ba_3Lu_2B_6O_{15}$: Ce^{3+},Tb^{3+} phosphor for near-UV-pumped white light-emitting diodes. *J. Alloy. Compd.* **2019**, *787*, 865−871.
(30) Annadurai, G.; Li, B.; Devakumar, B.; Guo, H.; Sun, L.; Huang, X. Synthesis, structural and photoluminescence properties of novel orange-red emitting $Ba_3Y_2B_6O_{15}$: Eu^{3+} phosphors. *J. Lumin.* **2019**, *208*, 75−81.
(31) Kolesnikov, I. E.; Bubnova, R. S.; Povolotskiy, A. V.; Biryukov, Y. P.; Povolotckaia, A. V.; Shorets, O. Y.; Filatov, S. K. Europium-activated phosphor $Ba_3Lu_2B_6O_{15}$: Influence of isomorphic substitution on photoluminescence properties. *Ceram. Int.* **2021**, *47*, 8030−8034.
(32) Shannon, R. D. Revised effective ionic radii and systematic studies of interatomic distances in halides and chalcogenides. *Acta Crystallogr., Sect. A: Cryst. Phys., Diffr., Theor. Gen. Crystallogr.* **1976**, *32*, 751−767.
(33) Zhao, S.; Yao, J.; Zhang, G.; Fu, P.; Wu, Y. $Ba_3Y_2B_6O_{15}$, a novel cubic borate. *Acta Crystallogr., Sect. C: Struct. Chem.* **2011**, *67*, i39−i41.
(34) Hoefdraad, H. E. Charge-transfer absorption band of Eu^{3+} in oxides. *J. Solid State Chem.* **1975**, *15*, 175−177.
(35) Blasse, G.; Bril, A.; Nieuwpoort, W. C. On the Eu^{3+} fluorescence in mixed metal oxides: Part I—The crystal structure sensitivity of thr intensity ratio of electric and magnetic dipole emission. *J. Phys. Chem. Solids* **1966**, *27*, 1587−1592.
(36) Binnemans, K.; Gorller-Walrand, C. Application of the Eu^{3+} ion for site symmetry determination. *J. Rare Earths* **1996**, *14*, 173−180.
(37) Ding, W.; Liang, P.; Liu, Z. Luminescence properties in relation to controllable morphologies of the $InBO_3$: Eu^{3+} phosphor. *Mater. Res. Bull.* **2017**, *94*, 31−37.
(38) Lu, Z.; Wang, J.; Tang, Y.; Li, Y. Synthesis and photoluminescence of Eu^{3+}-doped $Y_2Sn_2O_7$ nanocrystals. *J. Solid State Chem.* **2004**, *177*, 3075−3079.
(39) Han, B.; Liu, B.; Zhang, J.; Shi, H. Luminescence properties of novel Ba_2MgWO_6: Eu^{3+} and g-C_3N_4/Ba_2MgWO_6: Eu^{3+} phosphors. *Optik* **2017**, *131*, 764−768.
(40) Ströbele, M.; Dolabdjian, K.; Enseling, D.; Dutczak, D.; Mihailova, B.; Jüstel, T.; Meyer, H. J. Luminescence matching with the sensitivity curve of the human eye: Optical ceramics $Mg_{8-x}M_x(BN_2)_2N_4$ with M = Al (x = 2) and M = Si (x = 1). *Eur. J. Inorg. Chem.* **2015**, *2015*, 1716−1725.
(41) Yadav, R. S.; Dutta, R. K.; Kumar, M.; Pandey, A. C. Improved color purity in nano-size Eu^{3+}-doped YBO_3 red phosphor. *J. Lumin.* **2009**, *129*, 1078−1082.
(42) Han, B.; Li, P.; Zhang, J.; Shi, H. High color purity orange-emitting $KBaBP_2O_8$: Eu^{3+} phosphor: Synthesis, characterization and photoluminescence properties. *J. Lumin.* **2014**, *155*, 15−20.
(43) Schaik, W. V.; Poort, S. H. M.; Schlotter, J. J. H.; Dorrestijn, E.; Blasse, G. Influence of impurities on the luminescence quantum efficiency of the lamp phosphor (Ce, Gd, Tb)MgB_5O_{10}. *J. Electrochem. Soc.* **1994**, *141*, 2201−2207.
(44) Blasse, G. Energy transfer in oxidic phosphors. *Phys. Lett. A* **1968**, *28*, 444−445.
(45) Buijs, M.; Blasse, G. One-dimensional energy migration in $EuMgB_5O_{10}$. *Chem. Phys. Lett.* **1985**, *113*, 384−386.
(46) Ju, G.; Hu, Y.; Wu, H.; Yang, Z.; Fu, C.; Mu, Z.; Kang, F. A red-emitting heavy doped phosphor $Li_6Y(BO_3)_3$: Eu^{3+} for white light-emitting diodes. *Opt. Mater.* **2011**, *33*, 1297−1301.
(47) Li, J.; Liang, Q.; Cao, Y.; Yan, J.; Zhou, J.; Xu, Y.; Dolgov, L.; Meng, Y.; Shi, J.; Wu, M. Layered structure produced non-concentration quenching in a novel Eu^{3+}-doped phosphor. *ACS Appl. Mater. Interfaces* **2018**, *10*, 41479−41486.
(48) Fouassier, C.; Saubat, B.; Hagenmuller, P. Self-quenching of Eu^{3+} and Tb^{3+} luminescence in $LaMgB_5O_{10}$: A host structure allowing essentially one-dimensional interactions. *J. Lumin.* **1981**, *23*, 405−412.
(49) Mi, R.; Zhao, C.; Xia, Z. Synthesis, structure, and tunable luminescence properties of novel $Ba_3NaLa(PO_4)_3F$: Eu^{2+},Mn^{2+} phosphors. *J. Am. Ceram. Soc.* **2014**, *97*, 1802−1808.
(50) Vu, T. H. Q.; Bondzior, B.; Stefańska, D.; Miniajluk, N.; Dereń, P. J. Synthesis, structure, morphology, and luminescent properties of Ba_2MgWO_6: Eu^{3+} double perovskite obtained by a novel co-precipitation method. *Materials* **2020**, *13*, 1614.
(51) Korte, S.; Jüstel, T. On the photoluminescence of $InBO_3$ and $TbBO_3$ doped by Eu^{3+} and Ce^{3+}. *Mater. Res. Bull.* **2018**, *104*, 27−37.
(52) Riedel, E. P. Effect of temperature on the quantum efficiency of Eu+3 flourescence in Y_2O_3, $ScBO_3$ and $LaBO_3$. *J. Lumin.* **1970**, *1−2*, 176−190.
(53) den Engelsen, D.; Harris, P.; Ireland, T.; Silver, J. Cathodoluminescence of nanocrystalline Y_2O_3: Eu^{3+} with various Eu^{3+} concentrations. *ECS J. Solid State Sci. Technol.* **2015**, *4*, R1−R9.
(54) Chen, Y.; Yu, B.; Gou, J.; Liu, S. F. Zero-thermal-quenching and photoluminescence tuning with the assistance of carriers from defect cluster traps. *J. Mater. Chem. C* **2018**, *6*, 10687−10692.
(55) Lin, C. C.; Tsai, Y. T.; Johnston, H. E.; Fang, M. H.; Yu, F.; Zhou, W.; Whitfield, P.; Li, Y.; Wang, J.; Liu, R.; Attfield, J. P. Enhanced photoluminescence emission and thermal stability from introduced cation disorder in phosphors. *J. Am. Chem. Soc.* **2017**, *139*, 11766−11770.
(56) Li, B.; Wang, S.; Sun, Q.; Lu, C.; Guo, H.; Huang, X. Novel high-brightness and thermal-stable $Ca_3Gd(AlO)_3(BO_3)_4$: Eu^{3+} red phosphors with high colour purity for NUV-pumped white LEDs. *Dyes Pigm.* **2018**, *154*, 252−256.
(57) Sakthivel, T.; Annadurai, G.; Vijayakumar, R.; Huang, X. Synthesis, luminescence properties and thermal stability of Eu^{3+}-activated $Na_2Y_2B_2O_7$ red phosphors excited by near-UV light for pc-WLEDs. *J. Lumin.* **2019**, *205*, 129−135.
(58) Vijayakumar, R.; Devakumar, B.; Annadurai, G.; Guo, H.; Huang, X. Novel high color purity and thermally stable Eu^{3+} ions activated $Ba_2Gd_5B_5O_{17}$ red emitting phosphor for near-UV based WLEDs. *Opt. Mater.* **2018**, *84*, 312−317.
(59) Patwardhan, M. A.; Kohale, R. L.; Jumale, R. K.; Khapre, S. A.; Joshi, R. K.; Yerpude, A. N. Determination of Judd-Ofelt parameters

https://doi.org/10.1021/acs.inorgchem.5c03366
Inorg. Chem. 2025, 64, 18588−18598

for $LiGd_{2-X}Y_x$: Eu^{3+} O_3 nanophosphor synthesis by combustion method with glycine as fuel for near UV light emitting diode. *Luminescence* **2025**, *40* (3), No. e70129.

https://doi.org/10.1021/acs.inorgchem.5c03366
Inorg. Chem. 2025, 64, 18588−18598